Current Biology, Volume *26*

Supplemental Information

Architecture and Connectivity Govern Actin Network Contractility

Hajer Ennomani, Gaëlle Letort, Christophe Guérin, Jean-Louis Martiel, Wenxiang Cao, François Nédélec, Enrique M. De La Cruz, Manuel Théry, and Laurent Blanchoin

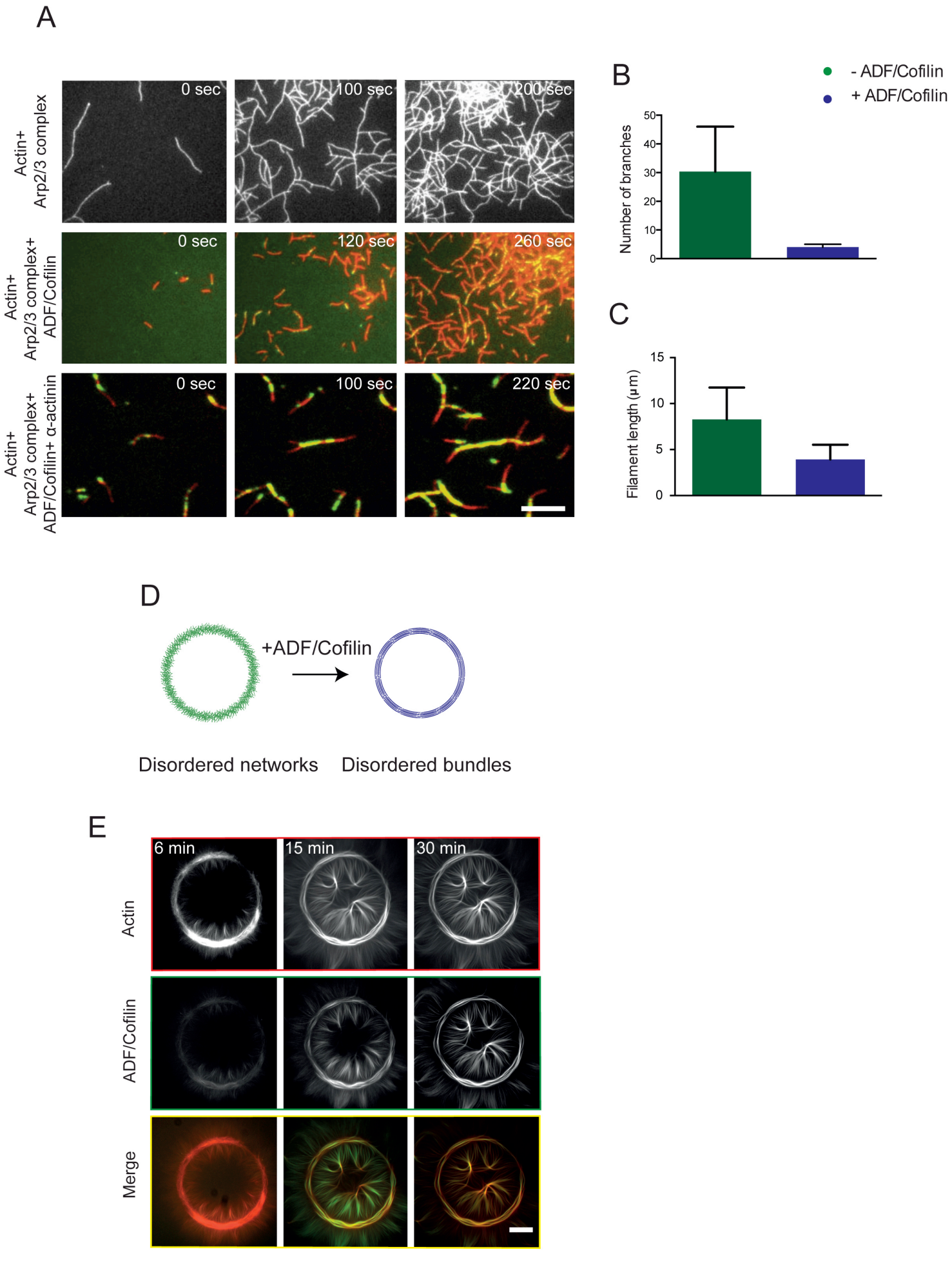
A
Actin+
Arp2/3 complex
0 sec
100 sec
200 sec
Actin+
Arp2/3 complex+
ADF/Cofilin
0 sec
120 sec
260 sec
Actin+
Arp2/3 complex+
ADF/Cofilin+ α-actinin
0 sec
100 sec
220 sec
B
- ADF/Cofilin
+ ADF/Cofilin
Number of branches
50
40
30
20
10
0
C
Filament length (μm)
15
10
5
0
D
+ADF/Cofilin
Disordered networks
Disordered bundles
E
6 min
15 min
30 min
Actin
ADF/Cofilin
Merge

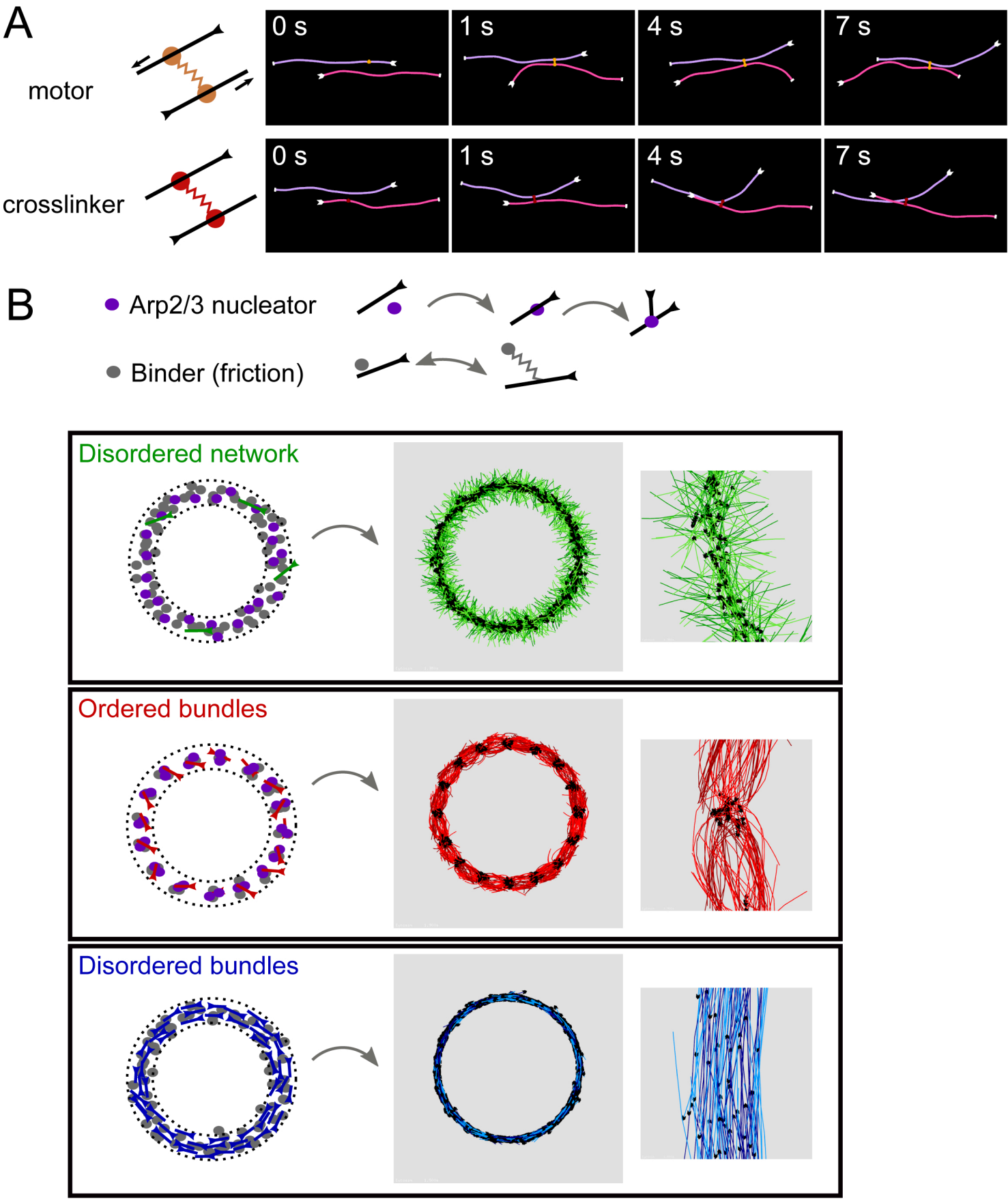
A
motor
crosslinker
0 s
1 s
4 s
7 s
0 s
1 s
4 s
7 s
B
Arp2/3 nucleator
Binder (friction)
Disordered network
Ordered bundles
Disordered bundles

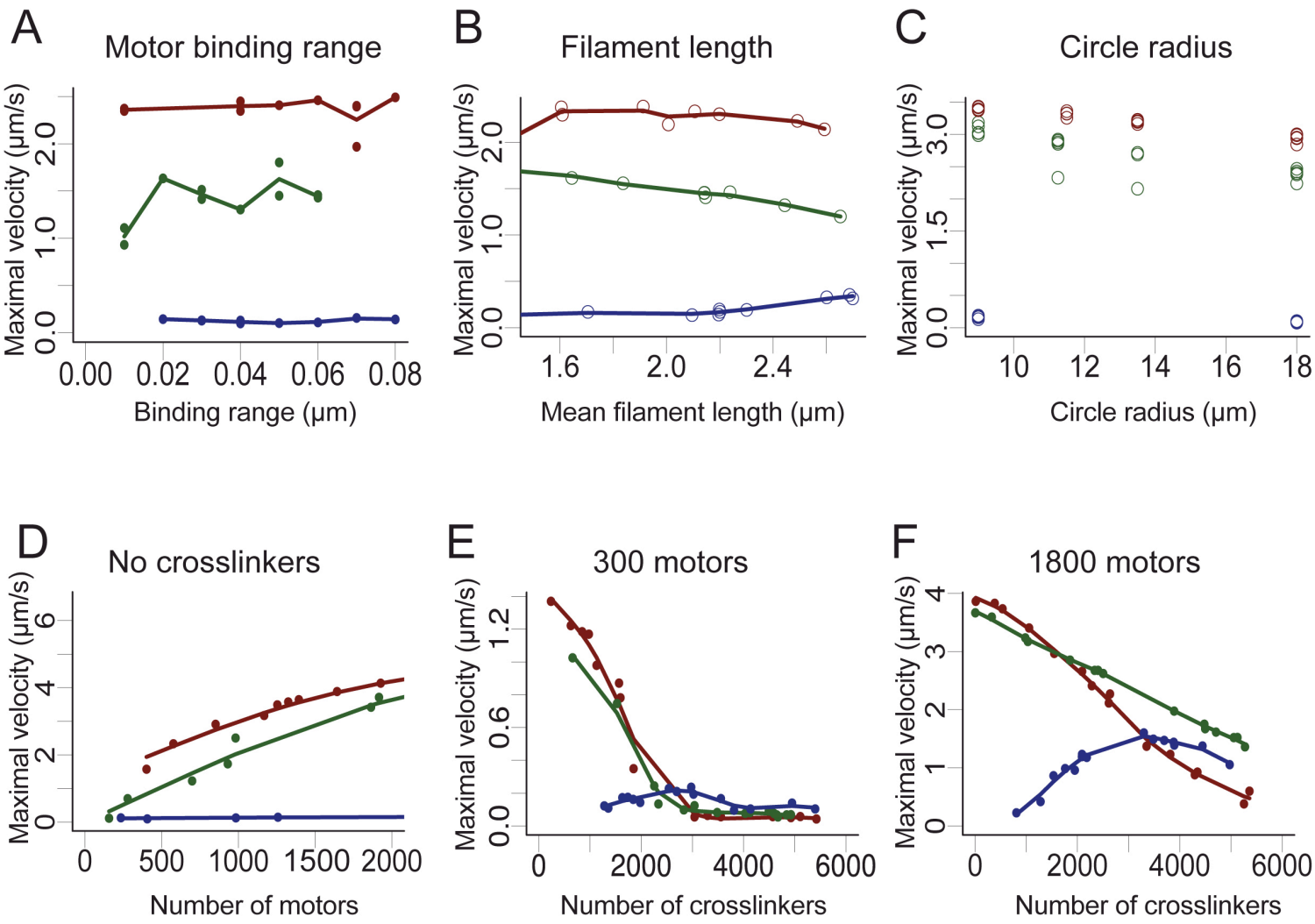
A
Motor binding range
Maximal velocity (µm/s)
0.0
1.0
2.0
0.00
0.02
0.04
0.06
0.08
Binding range (µm)
B
Filament length
Maximal velocity (µm/s)
0.0
1.0
2.0
1.6
2.0
2.4
Mean filament length (µm)
C
Circle radius
Maximal velocity (µm/s)
0.0
1.5
3.0
10
12
14
16
18
Circle radius (µm)
D
No crosslinkers
Maximal velocity (µm/s)
0
2
4
6
0
500
1000
1500
2000
Number of motors
E
300 motors
Maximal velocity (µm/s)
0.0
0.6
1.2
0
2000
4000
6000
Number of crosslinkers
F
1800 motors
Maximal velocity (µm/s)
0
1
2
3
4
0
2000
4000
6000
Number of crosslinkers

A

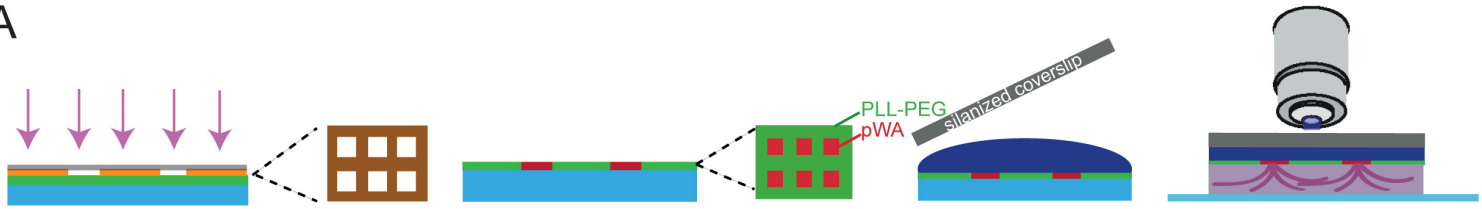

Deep ultraviolet exposure through photomask

pWA coating on exposed region

Transfer of the pWA on polyacrylamide gel

Traction force microscopy

B

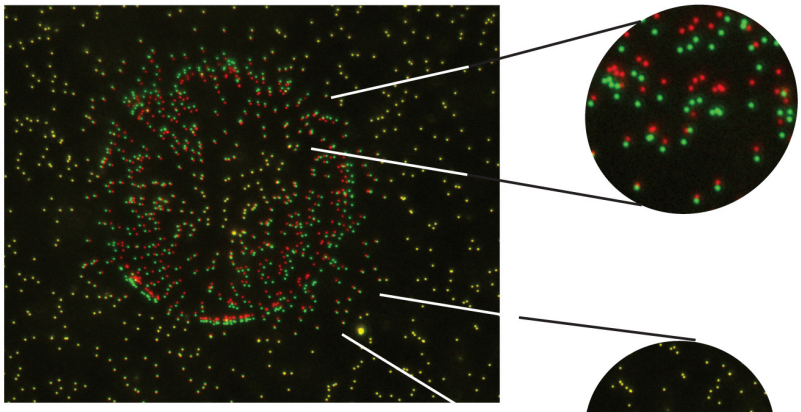

Overlay of picture before (green) and after (red) beads displacement.

C

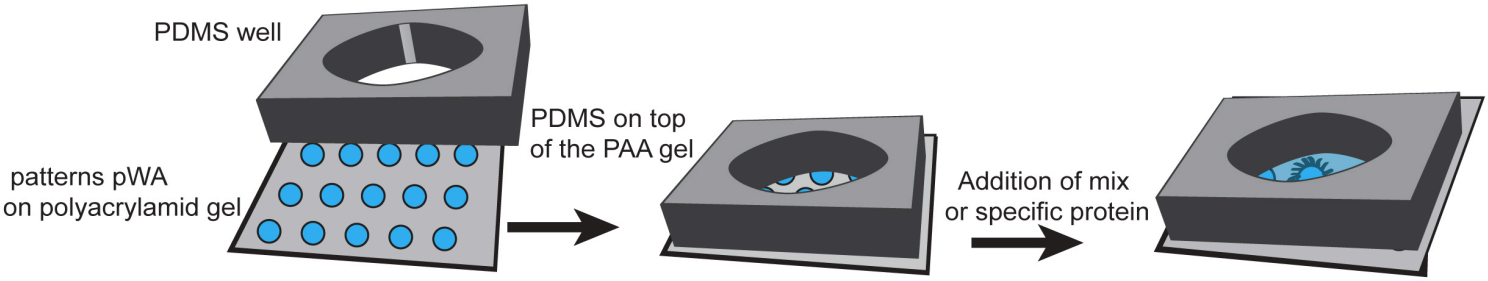

Figure S1. Related to Figure 1. ADF/cofilin debranching activity allows the transition between branched actin network and disordered actin fibers

(A) Montage of time-lapse total internal reflection fluorescence microscopy (TIRFm) images showing the time course of assembly of 0.8 μM Alexa-568-labeled actin with 50 nM Arp2/3 complex (top panel), in presence of 200 nM Alexa-488-cofilin (middle panel) or 200 nM Alexa-488-cofilin and 80nM α-actinin (bottom panel). Alexa-568-actin filaments and Alexa-488-ADF/Cofilin were color-coded in red and green respectively, and the ADF/Cofilin-decorated filament segments are represented in yellow in the merged images. Scale bar 10μm
(B) Quantification of the effect of ADF/Cofilin on branched actin network.
(C) Quantification of the effect of severing by ADF/Cofilin on the average length of actin filaments.
(D) Schematic representation of the reorganization of the actin filaments on a ring pattern upon addition of ADF/Cofilin.
(E) Time-lapse fluorescence microscopy of the effect of ADF/Cofilin on branched actin filaments nucleated on a micropatterned ring (actin monomers are labeled with Alexa-568 and ADF/Cofilin is labeled with Alexa-488). Top row represents the actin signal (red), middle row represents the ADF/Cofilin signal (green) and bottom row is the merge of the two signals. Scale bar = 25 μm

Figure S2. Related to Figures 2 and 4. Main features of the simulations

(A) (Top) Schematic view of a myosin VI-like motor entity acting between two antiparallel filaments. The two identical heads move toward the pointed ends of the filaments and slide the filaments apart (right).
(A) (Bottom) Schematic view of α-actinin like entity connecting two antiparallel filaments. The two static heads are linked by a spring like (Hookean) force term, constraining the filaments in their motions.
(B) (Top) Arp2/3 and binders are used to create the desired actin architecture. Arp2/3 complex-like entities induce branching from the side of an existing filament. Binder entities are anchored to a fixed position on the substrate, and can dynamically bind and unbind to filament. They simulate friction between the filaments and the pattern.
(B) (Bottom) The disordered branched network (green) is created by initially distributing Arp2/3 complex-like entities, binders and a few short filament seeds on a ring (left panel). Actin filament assembly and branching are simulated with artificially high rates for ~1 second to obtain the disordered branched network.
The rings containing a series of antiparallel bundles (red) are created by initially putting 16 dots of Arp2/3 complex-like entities, binders and few primer filaments. During the fast growth phase, actin filaments are constrained between two circles to keep them circularly oriented. Actin filaments growing from the pattern dots meet in an anti-parallel fashion.
The disordered bundle rings are created by adding preformed actin filaments tangentially to the circle, randomly clockwise or anticlockwise with equal probabilities. Binders are also distributed randomly on the ring. Light and dark shades of blue indicates opposite orientations of the actin filaments. The rightmost column contains a detailed view of the corresponding rings.

Figure S3. Related to Figure 2. Main parameters affecting the simulation of ring deformation in absence of crosslinkers

(A) Effect of the motor binding range on ring deformation for the different architectures. Disordered network (green), ordered bundles (red) and disordered bundles (blue).
(B) Effect of the filament length on ring deformation for the different architectures.
(C) Effect of the pattern radius on ring deformation for the different architectures. When the radius of the ring is increased, all the other quantities (number of motor, filaments) increase proportionally to maintain constant density along the ring.
(D) Effect of the number of motors on ring deformation for the different architectures.
(E) Effect of the number of crosslinkers in presence of 300 motors on ring deformation for the different architectures.
(F) Effect of the number of crosslinkers in presence of 1800 motors on ring deformation for the different architectures.

Figure S4. Related to Figure 6. Soft patterning method and setup for the sequential addition of components during an experiment of ring contraction on soft pattern

(A) Soft patterning: cartoon of the micropatterns on polyethylene glycol coated glass slide followed by their incubation with WASp-PWA to allow proteins adsorption to the micropatterned regions.

Polyacrylamide solution was added between the patterned pWA coverslip and a silanized coverslip for 20 minutes to allow the transfer of the protein from the hard to the soft substrate when the gel is fully polymerized.
(B) Overlay of beads signal before (green) and after (red) contraction illustrating beads displacement.
(C) Schematic representation of the PDMS well for dynamic experiment.

Supplemental Experimental Procedures

Protein expression and purification

Actin was purified from rabbit skeletal-muscle acetone powder. Actin was labeled on lysines with Alexa-568 according to [S1]. Arp2/3 complex was purified from bovine brain extracts [S2]. GST-pWA, ADF/Cofilin and human profilin were expressed and purified as described previously [S3, S4]. Double-headed (referred to as HMM) porcine myosin VI with bound calmodulin was purified from Sf9 cells by FLAG affinity chromatography [S5].

α-actinin: the pGex4T-1-ACTN4-6xHis construct was overexpressed in rosetta 2 DE3 pLys bacteria. The pellet was resuspended in a buffer containing 20 mM Tris pH 7.5, 150 mM NaCl, 1 mM DTT, 1 mM EDTA, 5% Glycerol and 1% Triton. After sonication, the lysate was centrifuged at 16000 rpm in a JA 25.50 rotor (beckman) for 30 minutes at 4°C. The supernatant was loaded onto a glutathione sepharose 4B resin (GE Healthcare) for 2 hours at 4°C. Elution was performed by adding 100 mM glutathione buffered in 20 mM Tris pH 7.5, 150 mM NaCl, 1 mM DTT, 1 mM EDTA. The eluted protein was loaded onto a Ni sepharose high performance resin (GE Healthcare) for 2 hours at 4°C. The resin was washed with a buffer containing 20mM Tris pH 7.5, 150mM NaCl, 1 mM DTT, 1 mM EDTA supplemented with 20 mM imidazole. Protein was eluted with 20 mM Tris pH 7.5, 150 mM NaCl, 1 mM DTT, 1 mM EDTA and 300 mM Imidazole and dialyzed against the storage buffer (20mM Tris pH 7.5, 150 mM NaCl, 1 mM DTT, 1 mM EDTA) over night at 4°C. Quality and concentration were estimated with a SDS-Page gel and ACTN4 was flash frozen in liquid nitrogen and then store at -80°C.

Semi-automated analysis of data of ring contraction rates

A specific semi-automated analysis of data was developed using ImageJ and MATLAB for the analysis of myosin induced-contraction of actin networks on patterned rings like described previously [S5].

Open chamber experiment

First, PDMS mixture was prepared by adding 10 g of DMS (Sylgard 184 Silicone Elastomer; Dow Corning) for each gram of curing agent. The mixture was degased for a minimum of 45 min, spread into a thin layer of about 5 to 10 mm, and heated for 20 min at 100 °C. PDMS was cooled down and stuck to the soft patterning coverslip after creating a well in the middle.

Traction force microscopy

The technique of polyacrylamide hydrogel micropatterning [S6] has been used to study the forces produced by the contractile actin organizations. A specific semi-automated analysis of data was developed using ImageJ as explained previously [S7].

Numerical simulations of architecture contractility

General features

Simulations were performed with the software Cytosim [S8] as previously described (Figure S2 and [S9]). In short, actin filaments are modeled as elastic fibers surrounded by an immobile viscous fluid, and their Brownian motion is calculated following Langevin dynamics. The filaments are of constant length, as simulating their assembly dynamics is not necessary to study the contractile behavior of a network. Steric interactions between filaments were not taken into account to simplify the model, as their effects were negligible on our system behavior. The crosslinkers are attached at fixed positions for simplicity (Figure S2A), during the first stage of the simulation during which the system is assembled. Molecular motors are made of two identical actin-binding motile “heads”. Each of them can bind and unbind stochastically to filaments and move along the filaments toward the pointed end. Motors diffuse when the two heads are unattached (Figure S2A). A motor with two

heads bound to different filaments creates a Hookean spring between these filaments. The motions of the attached heads toward the pointed end of the filament generate a contractile stress (Figure S2A). The Arp2/3 complexes also act as Hookean spring between the pointed end of one filament (daughter filament) and a random position along the mother filament, with an additional torque constraint to reproduce the characteristic angular branching (Figure S2B). Finally, Binders link the filament to random positions on the patterned area, to mimic the immobilization of actin on the patterned area (binders, Figure S2B). Attached binders are also represented as Hookean springs.

The main parameters used for simulating the objects are given in the Table.

Parameter	**Value**	**Description**
General		
Temperature	25 °C	In-vitro conditions. This defines the level of Brownian motion in the dynamics.
Viscosity	0.18 pN s / μm^2	In-vitro conditions (in the presence of methylcellulose)
Simulated time	80 s	With a time step of 10 ms
Pattern diameter	9 µm	
Actin filaments		
Persistence length	10 to 15 µm	From [S1, S10]
Length	see below	Filaments are of constant length
Molecular motor		
Binding rate	5 s^{-1}	Rate at which free myosin binds to actin filaments. This value was calculated from k_+ and the concentration of actin and myosin in the sample. (4.5-9 s^{-1}, from [S11])
Binding range	50 nm	Average myosin step size. The results were relatively insensitive within the range 20 to 80 nm (Fig S3A).
Unbinding force	3.65 pN	Typical "rupture" force required to detach myosin VI from actin filament [S12]. Detachment is modeled stochastically using Kramer's theory for its dependence on force: $w = w_0 \exp(\left\|\vec{f}\right\| / f_0)$
Maximal speed	v_m = 0.3 µm s^{-1}	Velocity of motor toward the pointed end, from [S13].
Stall force	f_s = 2 pN	Parameter of the linear force velocity relationship $v = v_m(1 + \vec{f} \cdot \vec{d} / f_s)$, that determines how motors are stopped by antagonistic force. From [S12, S14].
Stiffness	100 pN/µm	Elastic constant of the link between the 2 heads, empirical.
Length	0.03 µm	Link resting length, ~ myosin lever arm, [S11].
Crosslinker		
		Crosslinkers are created during an initial stage, and are static during the contraction phase.
Stiffness	100 pN/µm	Elasticity constant of the link between the two extremities, same as molecular motor stiffness
Length	40 nm	Link resting length, ~ α-actinin length, [S15].
Binders		
Binding rate	5 s^{-1}	Rate of attachment of a free binder to a filament. Empirical value
Binding range	30 nm	Distance of attachment. Empirical value
Unbinding rate	0.05 s^{-1}	Low detachment rate in the absence of force
Unbinding force	0.05 pN	Characteristic detachment force (see Kramer's theory above). A binder can easily be detached with a small force, which matches the experiments where rings detach from the substrate.
Stiffness	2 pN/µm	Elasticity of the Hookean spring

Disordered network		
	Number of filaments	1744
	Filament length (µm)	Between 0.95 and 1.25 uniformly distributed.
	Number of Arp2/3 entities	1569
	Number of binders	2000
Ordered fiber		
	Number of filaments	1200, this number is lower because the filaments are longer (see below)
	Mean filament length (µm)	Between 1.45 and 1.75 uniformly distributed
	Number of Arp2/3 entities	1152
	Number of binders	1360
Disordered fiber		
	Number of filaments	1744
	Mean filament length (µm)	Between 0.95 and 1.25 uniformly distributed
	Number of Arp2/3 entities	0
	Number of binders	2000

Table: The main parameters used during simulation.

Architecture simulations

The simulations are composed of two phases: during the first "growth" phase, the system is setup into the desired configuration to represent disordered networks, ordered and disordered bundles. Then crosslinkers (variable entities) and molecular motors (600 entities) are added to the actin organizations, and the system is simulated for 80 s. In this second phase, the behavior of the system is recorded and analyzed. The first phase is different for each network, but the second phase is identical in all cases.
To form a disordered branched network (Figure S2B, green), Arp2/3-like entities are distributed along the circular pattern, and primer filaments are randomly added. Nucleation and elongation occur during the first phase so that all the patterned area is covered with short, branched actin filaments.

To create a ring made of ordered bundles (Figure S2B, red), the Arp2/3-like entities and primer filaments are distributed over 16 discs of diameter 0.5 µm, regularly distributed on the ring pattern. They are also confined between two circles of radius R_1 =4.25 µm radius and R_2 =4.75 µm radius, to force them to cover a circular area corresponding to the experimental pattern. The confinement circles are removed for the second phase.

Disordered bundles (Figure S2B, blue) are generated by randomly distributed actin filaments of desired length on the pattern area. The parameters of the filaments are different for each architecture (Table) and are chosen to obtain the same total amount of linear polymerized actin on the ring (but the number of filaments and thus their average length vary for each architecture), and the same density of "binders" by patterned area.

Simulations analysis

The rate of contraction is defined as the maximal time-derivative of ring perimeter. Network connectivity is defined as the mean number of static links per actin filament: e.g. if one filament has one crosslinker bound and one Arp2/3 complex entity bound, its connectivity will be 2. The connectivity indicates how one filament is locally connected to its neighbors. Filaments are connected together by crosslinkers or the Arp2/3 complex in clusters (groups of filaments all connected together). The size of the largest cluster (or the fraction of filaments that are in the largest cluster) gives a measure of the overall connectivity of the actin organization (when the fraction is close to 1, all filaments are connected together, and when the fraction is close to zero, the network is disconnected). To evaluate the change in perimeter during ring contraction in the simulation, the radius of the network is calculated by averaging the distance of all the minus end of the filaments to their gravity centre.

Filaments buckling analysis

Filament curvature was calculated for each filament as the average of curvature, defined as the inverse of the radius defined by the configuration of each consecutive triplet of points that defines the filaments in the simulation:

$$\frac{1}{r} = \sqrt{\frac{1-\cos(\theta)}{2}}\ \frac{2}{seg}$$

where r is the local curvature radius, θ is the angle defined by the three consecutive points, and 'seg' is the segments length. The calculated curvatures are then averaged over all the filaments.

Infinite rigidity filaments

To simulate filaments with an infinite rigidity, we set the segmentation length of the filaments to 10 µm, thus well above the filament length. In this case, Cytosim only uses one segment (two points) to model a filament, which therefore is straight.

Variation of initial architecture's connectivity

To generate architectures configuration with different initial connectivity (without crosslinkers addition) for branched disordered networks and ordered bundles, which contain Arp2/3-like entities, we varied the number of Arp2/3-like entities and adjusted in accordance the number of "primers" filaments (unconnected filaments presents in the initial configuration) to maintain the total number of filaments constant. By decreasing the number of initial Arp2/3-like entities (thus increasing the number of independent clusters) we could obtain accordingly a low value (below 2) of the initial connectivity.

Supplemental References

S1. Isambert, H., Venier, P., Maggs, A.C., Fattoum, A., Kassab, R., Pantaloni, D., and Carlier, M.-F. (1995). Flexibility of actin filaments derived from thermal fluctuations. J. Biol. Chem. *270*, 11437-11444.

S2. Higgs, H.N., Blanchoin, L., and Pollard, T.D. (1999). Influence of the C terminus of Wiskott-Aldrich syndrome protein (WASp) and the Arp2/3 complex on actin polymerization. Biochemistry *38*, 15212-15222.

S3. Reymann, A.-C., Martiel, J.-L., Cambier, T., Blanchoin, L., Boujemaa-Paterski, R., and Théry, M. (2010). Nucleation geometry governs ordered actin networks structures. Nat. Mat. *9*, 827-832.

S4. Suarez, C., Roland, J., Boujemaa-Paterski, R., Kang, H., McCullough, B.R., Reymann, A.C., Guerin, C., Martiel, J.L., De la Cruz, E.M., and Blanchoin, L. (2011). Cofilin tunes the nucleotide state of actin filaments and severs at bare and decorated segment boundaries. Curr. Biol. *21*, 862-868.

S5. Reymann, A.-C., Boujemaa-Paterski, R., Martiel, J.-L., Guérin, C., Cao, W., Chin, H.F., De La Cruz, E.M., Théry, M., and Blanchoin, L. (2012). Actin Network Architecture Can Determine Myosin Motor Activity. Science *336*, 1310-1314.

S6. Vignaud, T., Ennomani, H., and Thery, M. (2014). Polyacrylamide hydrogel micropatterning. Methods Cell Biol. *120*, 93-116.

S7. Martiel, J.L., Leal, A., Kurzawa, L., Balland, M., Wang, I., Vignaud, T., Tseng, Q., and Thery, M. (2015). Measurement of cell traction forces with ImageJ. Methods Cell Biol. *125*, 269-287.

S8. Nedelec F., and Foethke D. (2007). Collective Langevin dynamics of flexible cytoskeletal fibers. New J Phys. *9*, 427.

S9. Letort, G., Politi, A.Z., Ennomani, H., Thery, M., Nedelec, F., and Blanchoin, L. (2015). Geometrical and mechanical properties control actin filament organization. PLoS Comput. Biol. *11*, e1004245.

S10. McCullough, B.R., Blanchoin, L., Martiel, J.L., and De la Cruz, E.M. (2008). Cofilin increases the bending flexibility of actin filaments: implications for severing and cell mechanics. J. Mol. Biol. *381*, 550-558.

S11. Robblee, J.P., Olivares, A.O., and de la Cruz, E.M. (2004). Mechanism of nucleotide binding to actomyosin VI: evidence for allosteric head-head communication. J. Biol. Chem. *279*, 38608-38617.

S12. Oguchi, Y., Mikhailenko, S.V., Ohki, T., Olivares, A.O., De La Cruz, E.M., and Ishiwata, S. (2008). Load-dependent ADP binding to myosins V and VI: implications for subunit coordination and function. Proc. Natl. Acad. Sci. USA *105*, 7714-7719.

S13. Rock, R.S., Rice, S.E., Wells, A.L., Purcell, T.J., Spudich, J.A., and Sweeney, H.L. (2001). Myosin VI is a processive motor with a large step size. Proc. Natl. Acad. Sci. USA *98*, 13655-13659.

S14. Altman, D., Sweeney, H.L., and Spudich, J.A. (2004). The mechanism of myosin VI translocation and its load-induced anchoring. Cell *116*, 737-749.

S15. Wachsstock, D.H., Schwarz, W.H., and Pollard, T.D. (1993). Affinity of alpha-actinin for actin filaments determines the structure and mechanical properties of actin filament gels. Biophys. J. *65*, 205-214.